Density-based molecular dynamics study of melting in a finite-sized cluster: Al_{13}

1998 J. Phys.: Condens. Matter 10 3309

(http://iopscience.iop.org/0953-8984/10/15/008)

J. Phys.: Condens. Matter **10** (1998) 3309–3320. Printed in the UK PII: S0953-8984(98)87876-4

Density-based molecular dynamics study of melting in a finite-sized cluster: Al_{13}

Abhijat Vichare and D G Kanhere†

Department of Physics, University of Pune, Pune 411 007, India

Received 26 September 1997, in final form 14 January 1998

Abstract. *Ab initio* molecular dynamical simulations have been performed to investigate the phenomenon of melting in a finite-size system, namely an Al_{13} cluster. Classical molecular dynamical simulations using Lennard-Jones potentials have shown that a coexistence region, where both solid-like and liquid-like behaviour is observed, exists over a range of total energy. Our density functional simulations on a metallic cluster aim at probing this coexistence region. Although our statistics is somewhat limited, we do find definite signatures of a coexistence region.

1. Introduction

During the last decade, there has been a great deal of interest in studying small aggregates of particles, since their properties are significantly different from those of the corresponding bulk materials. The impetus for studying cluster physics has come from the availability of a variety of experimental techniques for synthesizing and analysing such aggregates, which can be formed by using noble-gas, semiconducting, metallic and transition metal atoms [1].

One of the properties of particular interest is the thermal behaviour of clusters. Recently Berry and co-workers carried out extensive studies on the dynamics of Lennard-Jones clusters and presented evidence for solid-like–liquid-like transitions [2]. An interesting observation has been that of the presence of a coexistence region during such transitions. Their simulations showed that Ar_{13} clusters exhibit a temperature below which the solid form is stable, and a higher temperature above which the liquid form is stable. For any temperature in between these two, the two forms coexist. Although this transition from solid-like phase to liquid-like phase is not a 'phase transition' in a strict sense, it is loosely referred to as 'melting'. Such melting transitions have also been investigated for molecular, ionic and metallic clusters, in some cases experimentally [3]. Interestingly, the power spectra of potential energy fluctuations in the liquid state show $1/f$ behaviour over a wide range of frequency f [4].

Almost all of the molecular dynamical (MD) simulations carried out to probe the dynamics associated with melting reported so far have used the classical Lennard-Jones description for the atomic interactions. Although extensive density functional MD investigations have been carried out on the ground-state zero-temperature properties of small clusters, relatively few investigations have attempted to probe their thermal behaviour. Thus it is attractive to perform first-principles density functional MD simulations to determine

† E-mail: amv,kanhere@unipune.ernet.in.

0953-8984/98/153309+12$19.50

whether the solid–liquid coexistence energy range is a feature of LJ systems or whether it is generic to a certain class of finite-size systems. With the advent of the powerful Car–Parrinello technique [5], it has become feasible to perform such simulations, albeit for a short simulation timescale as compared to what can be studied in classical MD. However, a full orbital-based simulation can turn out to be prohibitively expensive. Recently, we [11] have developed and applied an orbital-free density-based MD (DBMD) technique for investigating ground states for a variety of clusters. This method approximates the kinetic energy functional in terms of charge density only, and speeds up the total energy calculations considerably. It may then be argued that the partial covalent character of the aluminium atom may not be within reach of the method used. We have demonstrated that the method is found to reproduce the ground-state geometries and their symmetries for simple metal-atom systems, for example Al_n, for $1 < n \leqslant 13$, and Al_nLi_m, where typically $m < n$ and $n_{max} = 13$ [11], when compared to the full Kohn–Sham-based geometries, with bond lengths within 6–8%. Hence, the DBMD technique is capable of capturing the essential physics at finite temperatures and is known to sustain long stable dynamical runs [6]. Thus it is ideally suitable for the present investigation.

In this paper, we describe the results of our simulations using DBMD for an Al_{13} cluster. It may be noted that the ground-state geometry of Al_{13} is the same as that of Ar_{13}, namely an icosahedron, which is reproduced accurately by the DBMD method. Furthermore, the Al_{13} cluster is a metal-atom cluster and is more strongly bonded than noble-gas systems. It may be noted that noble-gas systems are typically studied via classical simulations. Our methodology for studying the melting transitions is analogous to the one used by Jellinek and co-workers. Thus each simulation is carried out at a constant energy and the procedure is repeated for several values of the energy.

In the next section, section 2, we give a brief introduction to DBMD along with the simulation procedure. The results are presented in section 3 while section 4 presents the conclusions.

2. Density-based molecular dynamics

The total energy of a system consisting of N_a atoms and N_e interacting electrons, under the influence of an external field due to the nuclear charges at coordinates $\boldsymbol{R}_n$, can be written as a functional of the total electronic charge density $\rho(\boldsymbol{r})$ as

$$E[\rho(\boldsymbol{r}), \{\boldsymbol{R}_n\}] = T[\rho(\boldsymbol{r})] + E_{ext}[\rho(\boldsymbol{r})] + E_{xc}[\rho(\boldsymbol{r}) + E_c[\rho(\boldsymbol{r})] + E_{ii}[\rho(\boldsymbol{r}), \{\boldsymbol{R}_n\}] \tag{1}$$

where E_{xc} is the exchange–correlation energy, E_c is the electron–electron Coulomb interaction energy, E_{ext} is the electron–ion interaction energy and E_{ii} is the ion–ion interaction energy. The first term representing the kinetic energy functional $T[\rho]$ is approximated as

$$T[\rho(\boldsymbol{r})] = F(N_e)T_0[\rho(\boldsymbol{r})] + T_w[\rho(\boldsymbol{r})] \tag{2}$$

where T_{TF} is the Thomas–Fermi term, T_W is the gradient correction given by Weizsacker and the factor $F(N_e)$ is given by

$$F(N_e) = \left(1 - \frac{2}{N_e}\right)\left(1 - \frac{A_1}{N_e^{1/3}} + \frac{A_2}{N_e^{2/3}}\right) \tag{3}$$

with optimized parameter values $A_1 = 1.314$ and $A_2 = 0.0021$ [10]. This kinetic energy functional is known to describe well the response properties of the electron gas and has yielded very good polarizabilities for various atomic systems. It also provides an excellent representation of the kinetic energy of atoms. The total electronic energy for a fixed

geometry of atoms is minimized using the conjugate gradient technique [7] and the geometry minimization has been performed using the Car–Parrinello simulated-annealing strategy. All of the DBMD calculations were performed using only the local part of the Bachelet, Hamann and Schlüter pseudopotentials [8] and the exchange–correlation potential of Ceperley and Alder as interpolated by Perdew and Zunger [9].

We have used a periodically repeated unit cell of length 40 au with a FFT mesh size of $64 \times 64 \times 64$. Fourier space evaluations are performed by expanding the square-root charge density as

$$\tilde{\rho}(\boldsymbol{r}) = \sum_{G} \tilde{\rho}(\boldsymbol{G}) \mathrm{e}^{\mathrm{i}\boldsymbol{G}\cdot\boldsymbol{r}}. \tag{4}$$

The simulation procedure that we have used is essentially similar to the one given by Jellinek *et al*. The ground-state configuration of Al_{13} at $T = 0$ K is uniformly radially expanded by a few per cent of the radius in the ground state in order to increase the *total energy*. After one has obtained the ground-state charge density by conjugate gradient minimization, the system is 'released' to perform an unconstrained dynamics, i.e. *constant-total-energy* dynamics. The recorded trajectories are then analysed. All of the averages are performed in the standard fashion after discarding the requisite number of initial time instants which is of the order of a few thousands. The range of total energies from -2.2089 au to -2.1583 au, corresponding to expansions from 5% to 32%, is investigated, with a total of 21 constant-energy runs.

We use the entire Fourier mesh, yielding an energy cut-off of about 76 Ryd. A time step of 20 au is used to evolve the system for about 30 000 time steps. This amounts to a total simulation time of ten picoseconds. Further details of the simulation technique may be found in reference [11] and the references therein. All of the quantities are expressed in atomic units.

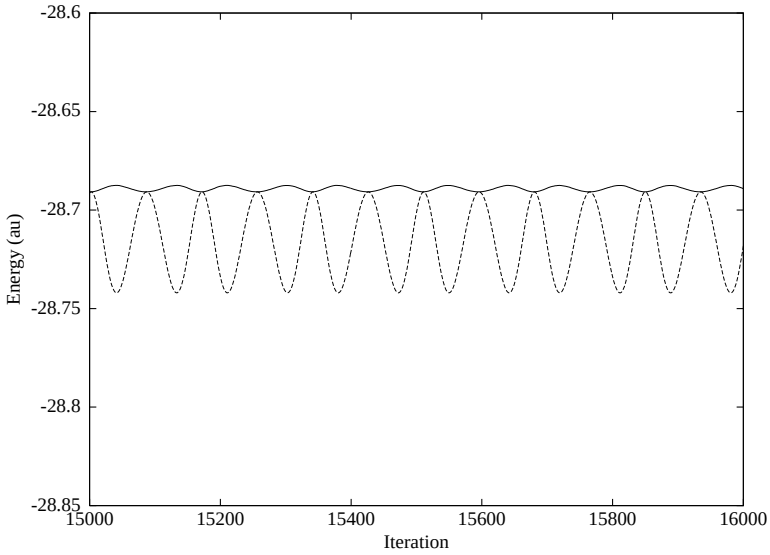

Figure 1. The total electronic energy (broken curve) and the grand total energy (continuous curve) as functions of the iteration number.

3. Results and discussion

In order to demonstrate the quality of the DBMD simulations, we show in figure 1 a plot of the grand total energy (solid curve) and the total electronic energy (dotted curve) as functions of time for the fixed energy value -2.2089 au, which corresponds to 5% expansion. The grand total energy, which is the sum of the total electronic energy, the ionic kinetic energy and the fictitious electronic kinetic energy, is a conserved quantity. The cluster is known to be in a solid-like region for this energy. For clarity, only a part of the simulation run is shown. The figure indicates that the grand total energy is constant to within 1 part in 10^4 au of energy and that the electrons follow the Born–Oppenheimer surface quite closely.

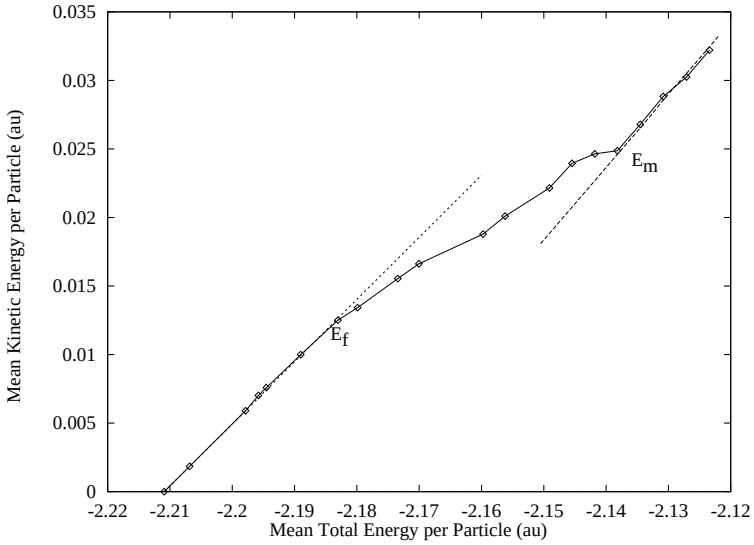

Figure 2. The caloric curve: the mean total energy per particle versus the mean kinetic energy per particle. The two energies E_f and E_m are marked.

Jellinek *et al* have presented evidence for the coexistence region by examining, among other results, the caloric curve, which represents the relationship between the mean kinetic energy per particle and the mean total energy per particle. We present our caloric curve in figure 2 for a wide range of energies corresponding to expansions from 5% to 32%. The short-term averaging has been carried out over 250 consecutive time steps, which averages out the vibrational motion. Evidently, the curve can be divided into three distinct regions: (a) the initial region, represented by a nearly straight line, which corresponds to low temperatures up to E_f; (b) the region above E_m, which exhibits a liquid-like behaviour; and (c) an intermediate region. The temperatures T_f and T_m corresponding to the energies E_f and E_m may be expressed as

$$T_i = \frac{2N}{3N-6}\frac{E_{kin}}{k} \tag{5}$$

where E_{kin} is the average kinetic energy per particle. The values calculated according to equation (5) are $T_f \simeq 2700$ K and $T_m \simeq 4600$ K [12].

The dotted lines in figure 2 are the extrapolations from the initial and final regions taken as approximate straight lines and would correspond to the bimodal distribution discussed by

Jellinek *et al*. In what follows, we will analyse these three energy regions and characterize them.

One of the parameters used to monitor the phase changes in the system is δ, the RMS bond-length fluctuation, which is defined as

$$\delta = \frac{2}{N(N-1)} \sum_{i<j} \frac{(\langle r_{ij}^2 \rangle_t - \langle r_{ij} \rangle_t^2)^{1/2}}{\langle r_{ij} \rangle_t} \tag{6}$$

where N is the number of particles in the system, r_{ij} is the distance between the ith and jth particles, and the time averages are calculated over the entire trajectory.

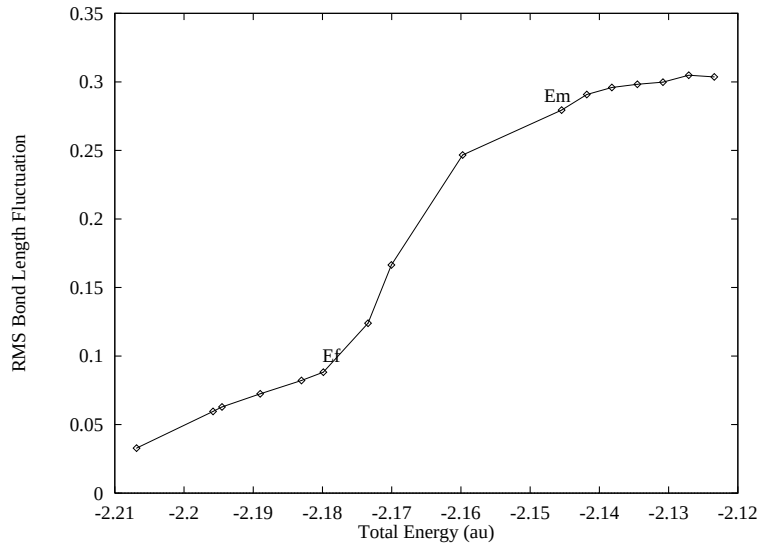

Figure 3. The RMS bond-length fluctuation, δ, versus the total energy.

In figure 3, we show δ as a function of the total energy of the system. It can be seen that the behaviour of δ reflects the three distinct regions seen in the caloric curve. In the region where the total energy $E < E_f$, δ has a small positive slope representing the thermal expansion of the solid-like region with values below 0.1. δ changes sharply from 0.1 to 0.3 in the second region where $E_f < E < E_m$. In the third region where $E > E_m$, it saturates at around a value of 0.3; this is the liquid-like diffusive region. Let us recall that the Lindemann criterion considers the region with δ less than 0.1 as being solid-like. Our results indicate that, in case of finite systems, crossing the Lindemann criterion line does represent the onset of the deviation from solid-like behaviour, and that the second region, where $0.1 < \delta < 0.3$, represents a coexistence phase.

In figure 4, we show the mean square displacements defined as

$$\langle \boldsymbol{r}^2(t) \rangle = \frac{1}{Nn_t} \sum_{j=1}^{n_t} \sum_{i=1}^{N} \left[\boldsymbol{r}_i(t_{0j} + t) - \boldsymbol{r}_i(t_{0j}) \right]^2 \tag{7}$$

for the three energies -2.2089 au (the solid-like region; curve a), -2.1905 au (the co-existence phase; curve b) and -2.1583 (the liquid-like region; curve c). These three energies are chosen as representative energies in the solid-like region, coexistence region and liquid-like region, respectively. Curve a, on this scale, is almost flat and is very close to the axis. In order to investigate the region around E_f in figure 4, we show the mean square

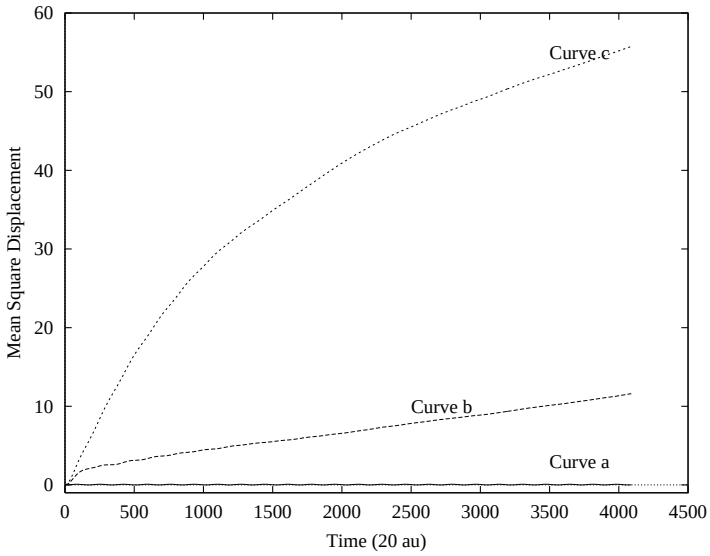

Figure 4. Mean square displacements versus the iteration number for the three regions: curve a: the solid-like region; curve b: the coexistence region; and curve c: the liquid-like region. On the scale used, curve a is almost along the x-axis.

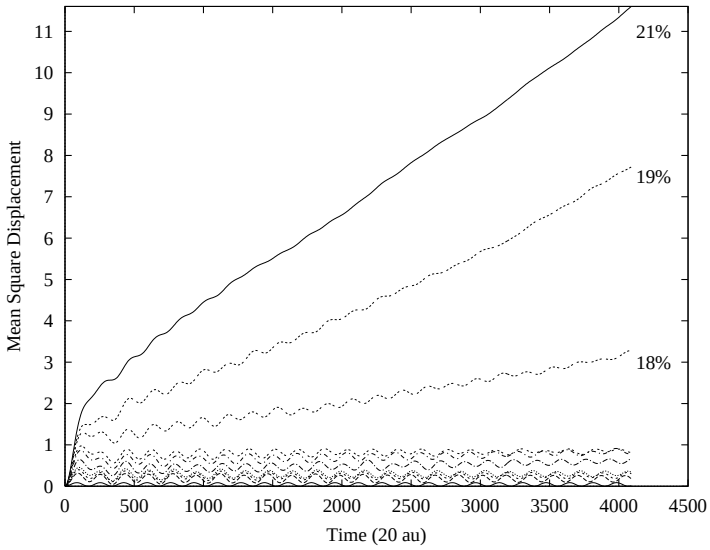

Figure 5. Mean square displacements versus the iteration number for expansions from 5% to 21%.

displacements for expansions from 5% to 21% in figure 5. Quite clearly, there is a change in the nature of the curve between expansions 16% and 18%. All of the curves below and including that for 16% expansion saturate very quickly around a maximum value of 1, which is characteristic of a solid-like behaviour. The curves for expansions above 16%, in the coexistence region, show a small gradual increase indicating at least a partially diffusive motion. As the temperature increases the slope also increases. In the molten region (curve c

of figure 4), the maximum root mean square displacement is about 7 au. This displacement is of the order of the cluster diameter and the diffusive motion is clearly evident.

We have also calculated the power spectrum, which provides information about the oscillation modes of the system. It is defined as

$$C(\omega) = 2\int_0^\infty C(t)\cos(\omega t)\ \mathrm{d}t \tag{8}$$

where $C(t)$ is the velocity autocorrelation function defined as

$$C(t) = \frac{\langle(\boldsymbol{v}(t_0+t) - \langle\boldsymbol{v}\rangle_t)\cdot(\boldsymbol{v}(t_0) - \langle\boldsymbol{v}\rangle_t)\rangle}{\langle(\boldsymbol{v}(t_0) - \langle\boldsymbol{v}\rangle_t)^2\rangle} \tag{9}$$

where $\langle\boldsymbol{v}\rangle_t$ is the average over the trajectory after discarding the requisite number of initial time instants.

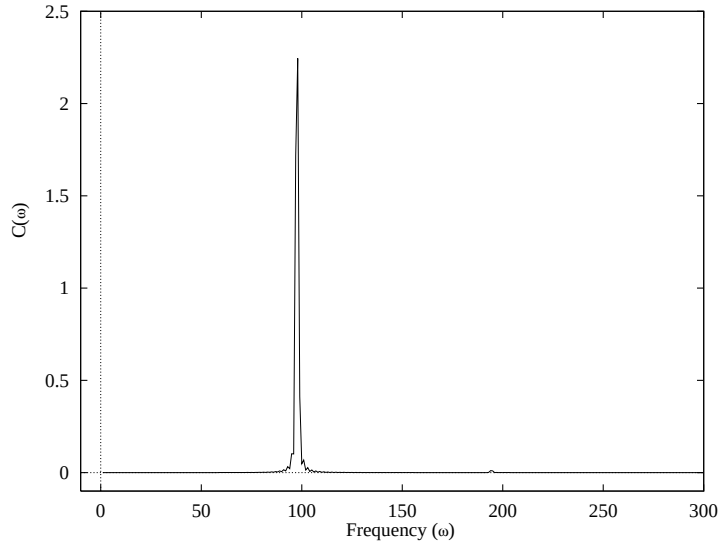

Figure 6. The power spectrum for the solid-like region. The energy corresponds to the energy of curve a in figure 4.

The power spectra for the three energy regions mentioned previously are presented in figures 6–8. Our curves show similar features to those seen by Jellinek *et al* [2]. Figure 6 shows a single-peaked spectrum corresponding to a breathing mode characteristic of solid-like behaviour. The $\omega = 0$ component is absent. Figure 7 shows a broad peak indicative of the softening of the modes, but still lacking a net diffusive motion. In contrast, a clear liquid-like behaviour is seen in figure 8 since there is no well defined sharp peak, indicating an absence of well defined vibrational modes. Furthermore, a non-zero $\omega = 0$ component is present.

An examination of an animation of the evolution of the cluster at different moments in time in the coexistence region reveals a fluctuating structure. The structure is not icosahedral, has high atomic mobilities and exhibits no ballistic motion.

Further insight can be gained by tagging a particle and studying the motion of its nearest neighbours during the evolution. It is expected that, in the solid phase, all of the particles will execute oscillatory (not necessarily harmonic) motion around the mean position and also all of the particles will remain in the same nearest-neighbour environment. For this

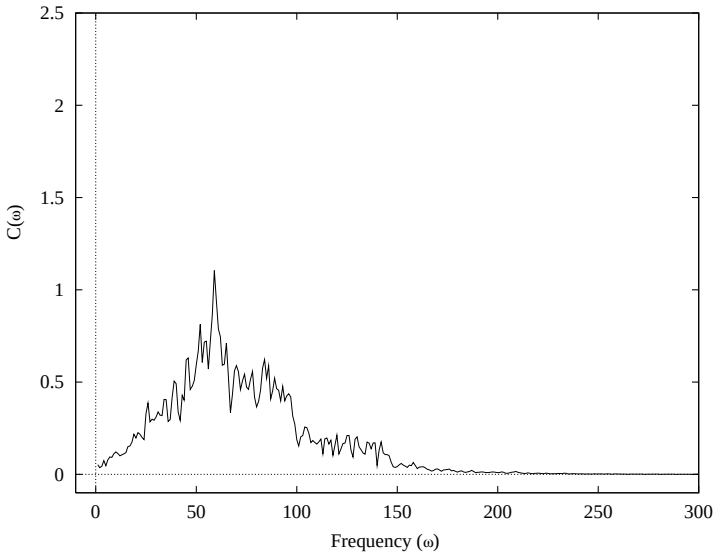

Figure 7. The power spectrum for the coexistence region. The energy corresponds to the energy of curve b in figure 4.

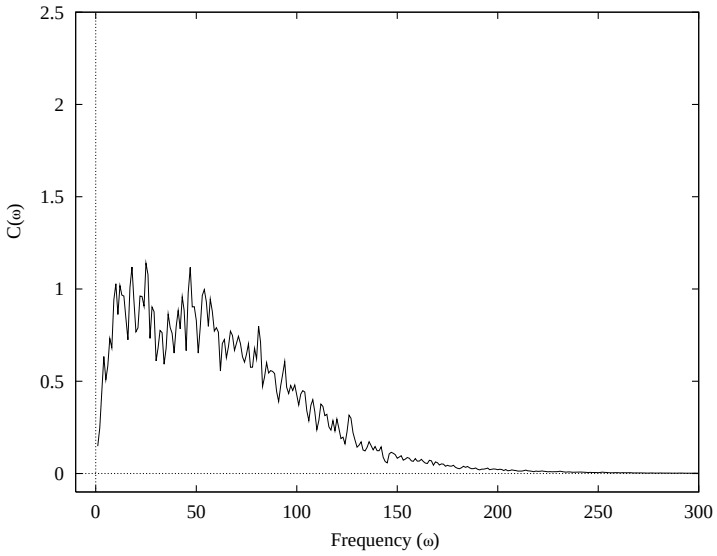

Figure 8. The power spectrum for the liquid-like region. The energy corresponds to the energy of curve c in figure 4.

purpose, we have focused on one particular particle on the surface. Its distance from three other particles, belonging to the first-, the second- and the third-nearest-neighbour shells, has been plotted as a function of time. This is shown in figures 9–11 for the three regions under consideration. The first shell is represented by the solid line labelled a, the second shell is represented by the dashed line labelled b and the third shell is represented by the dotted line labelled c. Clearly, in the solid-like region in figure 9, the particles are never exchanged between the shells. In figure 10, which shows the coexistence region, it can be

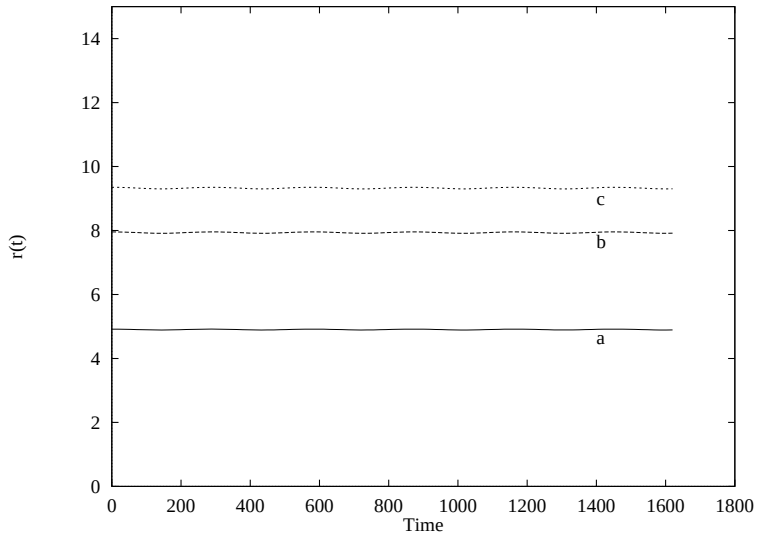

Figure 9. The nearest-neighbour distances from the tagged atom of the three particles as functions of the iteration number for the solid-like region. Every 100th iteration is plotted and further averaged over one cycle. Curve a (continuous curve): the atom in the first-nearest-neighbour shell; curve b (dashed curve): the atom in the second-nearest-neighbour shell; curve c (dotted curve): the atom in the third-nearest-neighbour shell.

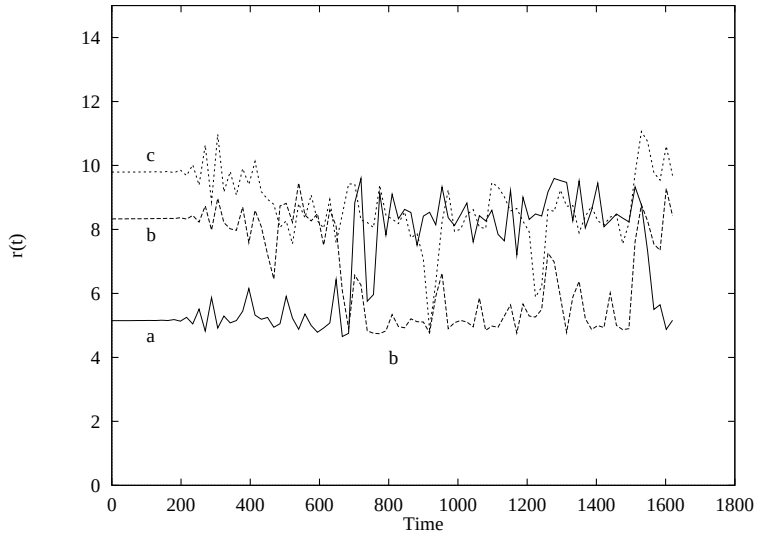

Figure 10. The nearest-neighbour distances from the tagged atom of the three particles as functions of the iteration number for the coexistence region. Every 100th iteration is plotted and further averaged over one cycle. Curve a (continuous curve): the atom in the first-nearest-neighbour shell; curve b (dashed curve): the atom in the second-nearest-neighbour shell; curve c (dotted curve): the atom in the third-nearest-neighbour shell.

seen that the particles from the first and second shells are exchanged but the shell structure is approximately preserved. For example, around the 700th time step the trajectories of the first- and the second-nearest neighbours have crossed and the first-nearest neighbour has

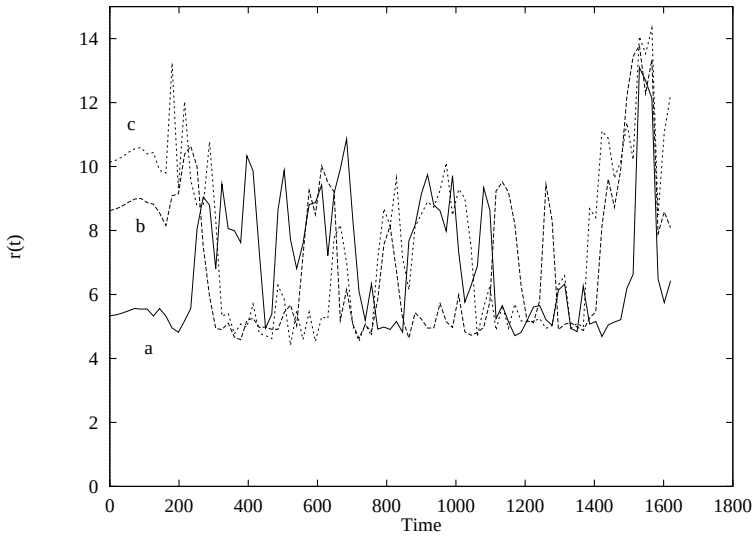

Figure 11. The nearest-neighbour distances from the tagged atom of the three particles as functions of the iteration number for the liquid-like region. Every 100th iteration is plotted and further averaged over one cycle. Curve a (continuous curve): the atom in the first-nearest-neighbour shell; curve b (dashed curve): the atom in the second-nearest-neighbour shell; curve c (dotted curve): the atom in the third-nearest-neighbour shell.

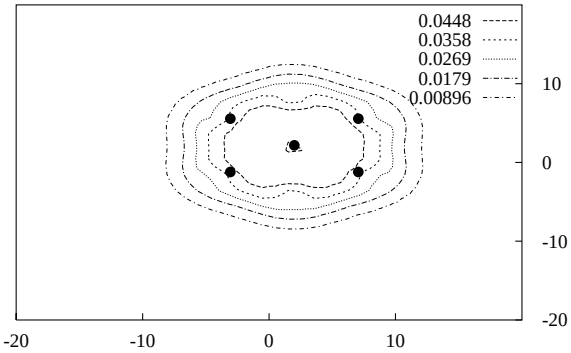

Figure 12. The electronic charge density in the $x = 0$ plane for 5% expansion. The scales along the y- and z-axes are in units of 0.8 au. The atomic sites are marked as filled circles.

become the second-nearest neighbour. Occasionally the third-nearest neighbour has diffused towards the first shell, as seen near the 900th time step. Completely diffusive motion of the particles is evident in figure 11, where a complete mixing of the trajectories is clearly seen.

Finally we compare the electronic charge density when the cluster is in a solid-like form with that when the cluster is in a liquid-like form. The 40 au unit cell is divided up using a $64 \times 64 \times 64$ mesh and the central region of about 40 mesh points is shown, to bring out the essential features of the charge density. The charge density outside this region is zero. A snapshot of the charge-density contours in the conveniently chosen $x = 0$ plane is shown in figure 12 for the solid at 5% expansion and having a cluster radius of 4.8 au. Also shown in the figure are the actual positions of the atoms, as filled circles, in the $x = 0$ plane. A small dip at the centre of the cluster and near the atomic sites,

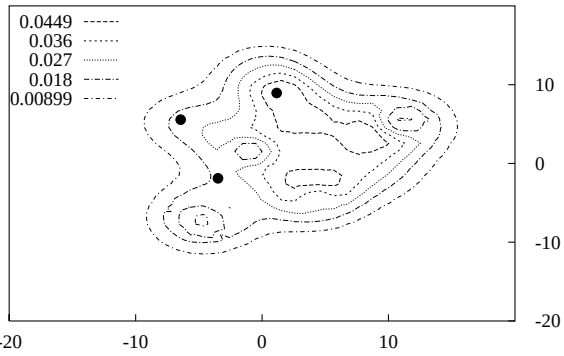

Figure 13. The electronic charge density in the $x = 0$ plane for 32% expansion. The scales along the y- and z-axes are in units of 0.8 au. The approximate atomic sites are marked as filled circles.

and a nearly symmetric charge density, are two features seen in the figure. The atomic positions suggest a near-rectangular contour profile since there are only five atoms on the yz-plane. Instead, a sixfold symmetric contour is seen because of the contribution due to four atoms above and below the $x = 0$ plane. In contrast, for the liquid-like cluster, the density does not show any particular symmetry, as the atoms have moved away considerably from their equilibrium positions. This can be seen in the instantaneous plot of the charge density shown in figure 13. Furthermore, the charge density in the liquid-like state is highly inhomogeneous although it is confined within a certain radius which is larger than that for the solid phase. It may be noted that in the case of the liquid-like charge-density plot, the atomic positions shown are of the three particles nearest to the $x = 0$ plane. The intermediate-density plots (not shown) resemble the liquid-like charge-density plots more than the solid-like charge-density plots.

4. Conclusions

It is evident from the discussion above that the system exhibits a coexistence region. The analysis of the caloric curve suggests two characteristic energies, E_f and E_m, such that below E_f the system is solid-like, while above E_m the system is liquid-like. Between these two energy regions the system is in a solid–liquid coexistence phase. This is corroborated by the RMS bond-length fluctuation curves and the power spectra. Analysis of the nearest-neighbour environment of a particular particle suggests a partial 'softening' of the rigid solid in the coexistence region, which gradually increases with total energy. Although the total simulation time is much less than the corresponding classical simulation times, we obtain clear signatures of the coexistence region.

Acknowledgments

It is a pleasure to acknowledge Vaishali Shah for extensive help and discussions. We also acknowledge Dr R Ramaswamy for a number of useful discussions. Partial financial assistance from the Department of Science and Technology (DST), Government of India, is gratefully acknowledged. One of us (AMV) gratefully acknowledges the research fellowship from CSIR, New Delhi. Thomas Williams and Colin Kelly are thanked for providing us with GNUplot.

References

[1] Jena P and Behera S N (ed) 1996 *Clusters and Nanostructured Materials* (New York: Nova Science)
Halicioglu T *et al* 1988 *Rep. Prog. Phys.* **51** 883
Andrea R P *et al* 1989 *J. Mater. Res.* **4** 704
Bonačič-Koutecky V *et al* 1991 *Chem. Rev.* **91** 1035
Brack M 1993 *Rev. Mod. Phys.* **65** 677

[2] Berry R S *et al* 1991 *Phys. Rev.* B **43** 10 647
Jena P *et al* 1992 *Phys. Rev. Lett.* **69** 1664
Vijaykumar *et al* 1993 *Phys. Rev. Lett.* **70** 2078
Wells D J and Berry R S 1994 *Phys. Rev. Lett.* **73** 2875
Beck T L, Leitner D M and Berry R S 1993 *J. Chem. Phys.* **89** 1681
Beck T L and Berry R S 1993 *J. Chem. Phys.* **88** 3910
Davis H L, Jellinek J and Berry R S 1987 *J. Chem. Phys.* **86** 6456
Jellinek J, Beck T L and Berry R S 1986 *J. Chem. Phys.* **84** 2783

[3] Buffat Ph and Borel J P 1976 *Phys. Rev.* A **13** 2287
Even *et al* 1989 *Phys. Rev. Lett.* **61** 140
Hahn M Y and Whetten R L 1988 *Phys. Rev. Lett.* **61** 1190
Schmidt M *et al* 1997 *Phys. Rev. Lett.* **79** 99

[4] Nayak S K, Ramaswamy R and Chakravarty C 1995 *Phys. Rev. Lett.* **74** 4181 and references therein

[5] Car R and Parrinello M 1985 *Phys. Rev. Lett.* **55** 685
Payne M C *et al* 1992 *Rev. Mod. Phys.* **64** 1045

[6] Pearson M, Smargiassi E and Madden P A 1993 *J. Phys.: Condens. Matter* **5** 3221

[7] Press W H, Flannery B P, Teukolsky S A and Vetterling W T 1987 *Numerical Recipes* (Cambridge: Cambridge University Press)

[8] Bachelet G B, Hamann D R and Schlüter M 1982 *Phys. Rev.* B **26** 4199

[9] Perdew J P and Zunger A 1981 *Phys. Rev.* B **23** 5048

[10] Ghosh S K and Balbas L C 1985 *J. Chem. Phys.* **83** 5778

[11] Nehete D, Shah V and Kanhere D G 1996 *Phys. Rev.* B **53** 2126
Shah V, Nehete D and Kanhere D G 1994 *J. Phys.: Condens. Matter* **6** 10 773
Shah V and Kanhere D G 1996 *J. Phys.: Condens. Matter* **8** L253
Shah V, Kanhere D G, Majumder C and Das G P 1997 *J. Phys.: Condens. Matter* **9** 2165

[12] These temperatures are too high as compared to the melting temperature of bulk Al (∼933 K). There is always a question as regards defining the temperature in the case of a microcanonical ensemble. Furthermore, we expect errors in determining T_m and T_f due to the poor statistics and due to the approximations used in the DBMD technique.